# High-resolution short-wave infrared hyperspectral characterization of alteration at the Sadiola Hill gold deposit, Mali, Western Africa

**Semyon Martynenko, Pekka Tuisku**
*Oulu Mining School, University of Oulu*

**Frank J.A. van Ruitenbeek**
*Faculty of Geo-Information Science and Earth Observation (ITC), University of Twente*

**Kim A.A. Hein**
*School of Geosciences, University of Witwatersrand*

**Abstract.** Sadiola Hill is an ~8 Moz gold deposit located in western Mali within a ca. 2200-2050 Ma tectonic window known as Kédougou-Kénieba inlier (KKI), exposing the Western African craton. The deposit is hosted in a metasedimentary package made up of impure carbonate rocks, wackes, and arenites intruded by three distinct igneous phases. A N-S-trending Sadiola shear zone, related to the regional Senegal-Mali shear zone, and NNE-trending third order fault splays acted as conduits for auriferous hydrothermal fluid flow. The deposit has undergone a complex poly-phase alteration history. Alteration assemblages related to gold mineralization consist of biotite-carbonate-quartz-sulphide. Other assemblages include calc-silicates, chlorite, white mica, scapolite, and tourmaline (Hein and Tshibubudze 2007; Cameron 2010; Masurel et al. 2017). Current research is aimed at characterising alteration at the mineral-scale, as well as assessment of cooling trend(s) and alteration footprint(s) with high-resolution short-wave infrared (SWIR) hyperspectral scanning. In addition to detailed mineralogical classification, changes in fluid chemical parameters are determined with variations in white mica, namely, the position of Al-OH bond in the SWIR range and white mica crystallinity. Furthermore, hydrothermal fluid chemistry is assessed with $Fe^{2+}$ content in carbonate group minerals**.** Protolith control on alteration expression is also investigated.

## 1 Introduction

Short-wave infrared (SWIR) hyperspectral imaging is a rapid and reliable technique for mineral identification. It has proven reliable at tracing hydrothermal fluid pathways in diverse range of deposit types, including orogenic gold systems in granite-greenstone terranes (van Ruitenbeek et al. 2012; Wang et al. 2017). In addition to precise identification of phyllosilicates and carbonates, SWIR spectroscopy identifies specific mineral parameters, such as Al-Si substitution in white mica, that correspond to physico-chemical changes of hydrothermal fluid (van Ruitenbeek et al. 2005). As such, it has become an effective vectoring tool in mineral exploration (Wang et al. 2017; Roache et al. 2011).

Current research investigates alteration assemblages within a world class Sadiola Hill gold deposit with SWIR hyperspectral imaging and conventional petrography. The study establishes paragenetic sequence and the number of hydrothermal events within the system. Spatial variation in the chemical composition of alteration minerals, and protolith control on alteration expression are also determined. The research is carried out on drill core samples from 6 diamond holes capturing the most representative alteration examples and is solely laboratory based. The core samples are scanned at medium (0.2mm pixel size) and high-resolution (26µm pixel size) scales. Paragenetic context of aspectral alteration mineralogy is determined with transmitted light microscopy. Spectral classes of the 26µm-pixel mineral maps are validated with petrographic observations and electron microprobe analyses.

## 2 Geologic setting

The West African craton exposed in the Kédougou-Kénieba inlier (KKI) is a unique Paleoproterozoic granite-greenstone belt as it contains a package of carbonate rocks of variable thickness not typical for other granite-greenstone belts worldwide. The KKI is comprised of series of volcano-plutonic belts and sedimentary basins dissected by two major regional faults, namely, the Main Transcurrent Zone (MTZ) and the Senegal-Mali Shear Zone (SMSZ). (Hein et al. 2015; Masurel et al. 2016).

Previous studies have revealed that Sadiola impure carbonates are overlain by a package of greywacke. Impure carbonates and detrital sediments have been intruded by three intrusive suites: early diorite, quartz feldspar porphyry, and late diorite. The rocks have undergone a regional mid-greenschist facies metamorphism (Hein and Tshibubudze 2007; Masurel et al., 2017).

Sadiola Hill records a complex brittle-ductile history evident from 3 distinct pre- and syn-mineralization deformation events as well as two smaller scale brittle events postdating gold deposition (Masurel et al. 2017). The key structural features of the Sadiola Hill deposit include the N-S-trending subvertical to vertical Sadiola shear zone, and associated NNE-trending fault splays. The Sadiola shear zone marks the major structural break

at Sadiola separating greywackes on the western side of the pit from marbles on the eastern side (Hein, 2008). Most notable is the $D_3$ deformation event that resulted in sinistral reactivation of Sadiola shear zone and the NNE-trending splays and was syn-genetic to auriferous hydrothermal fluid flow along these structures (Hein and Tshibubudze 2007; Cameron 2010; Masurel et al. 2017).

Complex poly-phase alteration history at Sadiola Hill consists of ore stage K-feldspar-biotite-carbonate-quartz-sulphide potassic alteration assemblages. Other assemblages include calc-silicates related to contact metamorphism during emplacement of igneous suits into the sedimentary package, as well as chlorite, white mica, scapolite, and tourmaline (Hein and Tshibubudze 2007; Cameron 2010; Masurel et al. 2017).

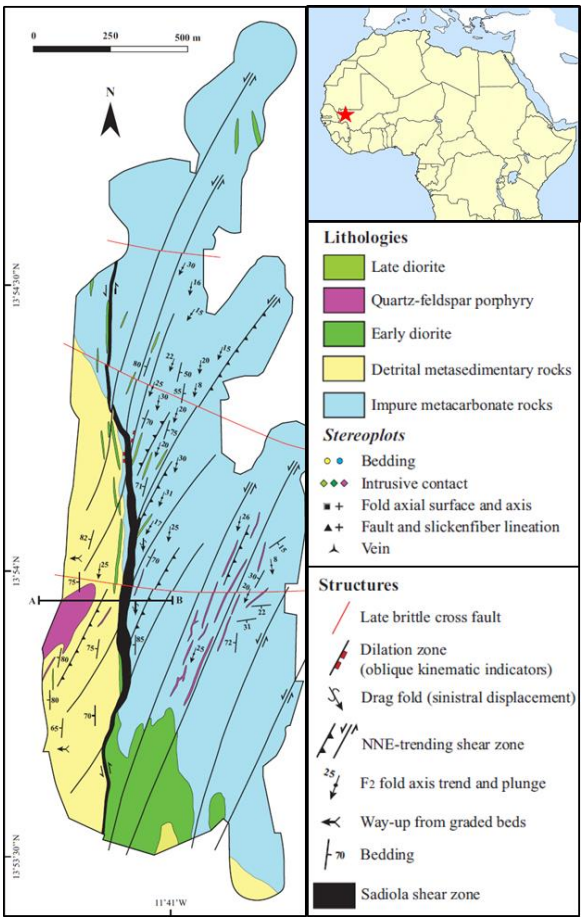


**Figure 1.** Sadiola Hill deposit geology after Masurel et al. (2017) Inset map shows deposit's location near Senegal-Mali border in Western Africa.

## 3 SWIR hyperspectral imaging

### 3.1 Background

SWIR hyperspectral imaging uses light reflection is 1000nm-2500nm range of the electromagnetic spectrum. Cation-OH, $H_2O$, $(CO_3)^{2-}$ in crystal structures reflect light in characteristic way producing diagnostic absorption features in the SWIR range (Clark 1999). White mica is characterized by absorption features positioned at 2200nm related to Al-OH bond, and 1900nm absorption feature corresponding to H-OH bond. Tschermak substitution of $Al^{3+}$ by $Fe^{2+}$ and $Mg^{2+}$ in muscovite crystal structure shifts position of Al-OH bond to longer wavelength (Dalm et al. 2017). Illite spectral response shows a subtle difference from white mica responses, as illite also has a deep absorption feature around 2200nm related to Al-OH bond as well as OH and H-OH bonds at 1400nm and 1900nm respectively (Agus 2011; Clark 1999).

Actinolite-tremolite series are distinguished by hydroxyl stretching and bending vibrations located near 2320nm and 2390nm as well as ferrous drop (Laukamp et al. 2012). Epidote-clinozoisite series distinguished from chlorites by 1550nm absorption feature. Spectral responses of chlorite are attributed Mg-OH and Fe-OH bonds at ~2340nm and ~2250nm respectively that shift to longer wavelengths with $Fe^{2+}$ substituting for $Mg^{2+}$. Carbonate group minerals (Figure 2) are identified by $(CO_3)^{2-}$ absorption band between 2300 and 2360nm combined with ferrous drop related to $Fe^{2+}$ substitution into crystal structure (Clark 1999; Roache et al. 2011).

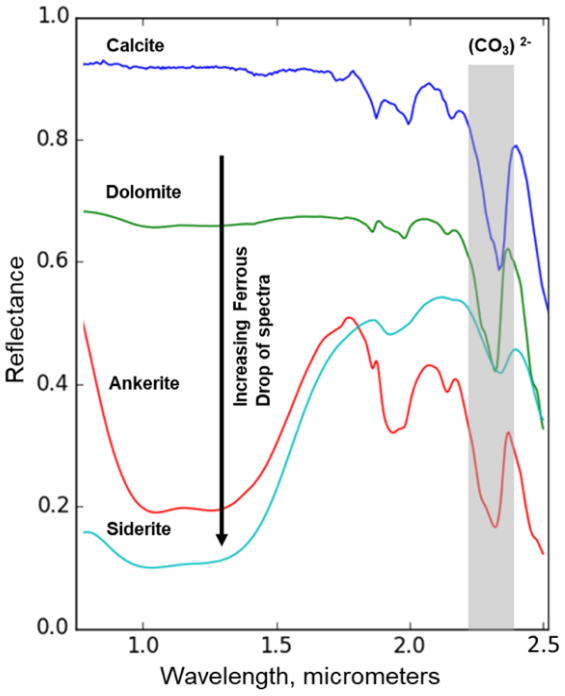


**Figure 2.** Spectral responses of carbonate group minerals in the SWIR range. Note ferrous drop in siderite and ankerite spectra. Figure generated from USGS spectral library version 7 after Kokaly et al. (2017).

### 3.2 Methodology

Hyperspectral scanning of drill core samples and offcut blocks was acquired at Faculty of Geo-Information Science and Earth Observation (ITC), University of Twente with Specim Hyperspectral camera at medium (0.26mm pixel size) and high-resolution (26µm pixel size). Data for each pixel is collected in x-, y-, and z-direction with x- and y-values of the pixel cube corresponding to length and width of a pixel within a

horizontally stationed sample. Z-values represent a stack of bands in the SWIR range with 12 nm spectral resolution, amounting for the total of 288 bands. Conversion of the raw data into calibrated hyperspectral images was done with hyperspectral python (hyppy), an in-house software developed in ITC. Calibrated images were converted into wavelength maps over 6 different ranges capturing depth and position of 1st, 2nd, and 3rd deepest absorption features. Decision trees are developed for project-specific mineralogy as matching algorithms between recorded bands to spectra from USGS spectral library. Polished thin sections were prepared from drill core samples scanned at high-resolution for one-to-one comparison of mineral maps to petrographic observations (van Ruitenbeek et al. 2017). Conventional transmitted light microscopy is added to the workflow to validate hyperspectral mineral maps and to add paragenetic constraints related to cross-cutting relationships and replacement textures to the interpretation. Exact stoichiometry of each spectral class is determined with electron microprobe.

Decision tree for muscovite and illite was constructed from combination of illite crystallinity, a ratio of depth of Al-OH absorption feature to the depth of water feature, and position of Al-OH bond. Overall, crystallinity was divided into 4 classes (>1, >2, >3, >4) based on observed variability in the samples. Position of Al-OH bond was assessed with 5nm breaks within Al-OH feature range.

Decision tree for carbonate group minerals has been developed based on $Fe^{2+}$ drop values and presence of $(CO_3)^{2-}$ absorption feature. Secondary Fe-OH feature near 2250nm was applied to filter out Fe-bearing phyllosilicates and epidote from carbonate classification. Position of the carbonate feature for ankerite, dolomite, and calcite were taken from the USGS spectral library and related studies (Kokaly et al. 2017).

Decision tree for classification of chlorites, calcic amphiboles, epidote and tourmaline was developed from combination of wavelength positions of the 1st and 2nd deepest absorption features in the 2100-2400nm range combined with position of the deepest features in 1850-2100nm and 1300-1600nm ranges. Ferrous drop was also utilized for tremolite-actinolite classification.

## 4 Preliminary results

Muscovite is more aluminous in igneous units in comparison to greywacke and impure carbonate reflecting availability of $Al^{3+}$. In cases where $Na^{+}$ is ubiquitous, e.g. tonalite unit, white mica composition changes to paragonite (Figure 4). Mineral-scale variations were also noted in muscovite. When muscovite replaces biotite, Al-OH feature shifts to longer wavelengths (~2210nm) consistent with incorporation of $Mg^{2+}$ from biotite into muscovite crystal structure. Illite crystallinity has a common trend of increasing inward into a vein and is also protolith dependent, with low crystallinity illites constrained to greywacke and muscovite to igneous units and impure carbonates.

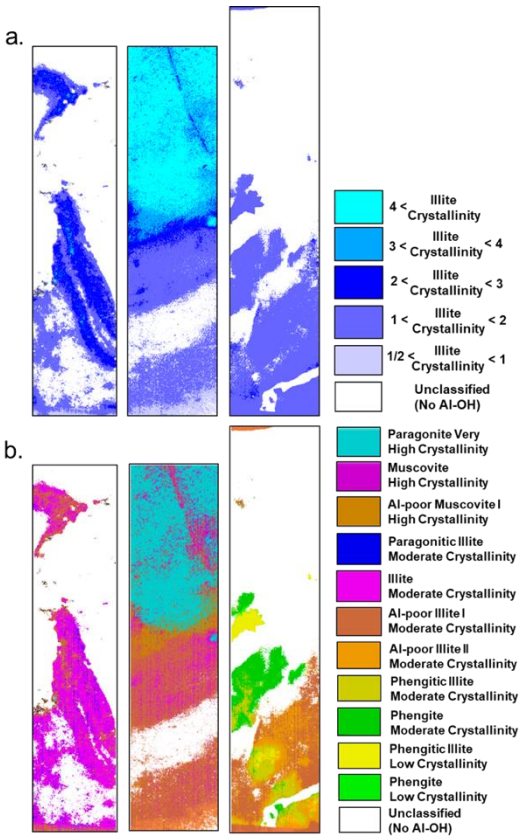


**Figure 4. a.** Illite crystallinity maps and **b.** corresponding illite/muscovite mineral maps of impure carbonate unit (left), tonalite-greywacke contact (centre), and greywacke (right) showing compositional variation in white mica. Map width is 10mm.

Ore-stage vein-controlled and pervasive carbonate alteration is represented by ferroan dolomite and ankerite in greywacke and diorite. Hyperspectral imaging of the least altered and umineralized samples of impure carbonate unit revealed it is dolomite-calcite dominant. In contrast, calcite is absent in the ore-zone impure carbonate samples. Hydrothermal calcite reoccurs in the system as late post-mineralization fracture-fill phase (Figure 5).

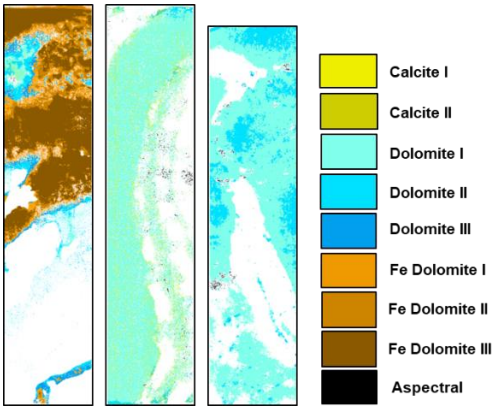


**Figure 5.** Carbonate mineral maps at 26µm pixel resolution showing variation and complexity of Sadiola Hill carbonate mineralogy. Ferroan dolomite vein cutting greywacke (left), least-altered (centre) and ore-zone (right) dolomite-calcite impure carbonate. Map width is 10mm.

Overall, alteration mineralogy at Sadiola Hill is variable and strongly protolith-dependent evident from both white mica and carbonate chemistry. Reactive folded argillaceous laminae within the impure carbonate acted as chemical trap for gold mineralization during the $D_3$ event. Biotite supplied iron for sulphidation reactions leading to pyrrhotite- arsenopyrite- chalcopyrite- sphalerite- pyrite- free gold precipitation (Figure 6). Dolomite-dominant laminae do not host sulphide-gold mineralization, but track $CO_2$ addition from auriferous fluid to impure carbonate host. Mineralization within greywacke is more sporadic with iron also sourced from biotite and is associated with patchy ferroan dolomite alteration, reflecting decomposition of silicates. Phlogopite occurs in all lithologic units in association with sulphides consistent with transition to Mg-rich silicate phase in response to iron consumption by sulphidation reactions.

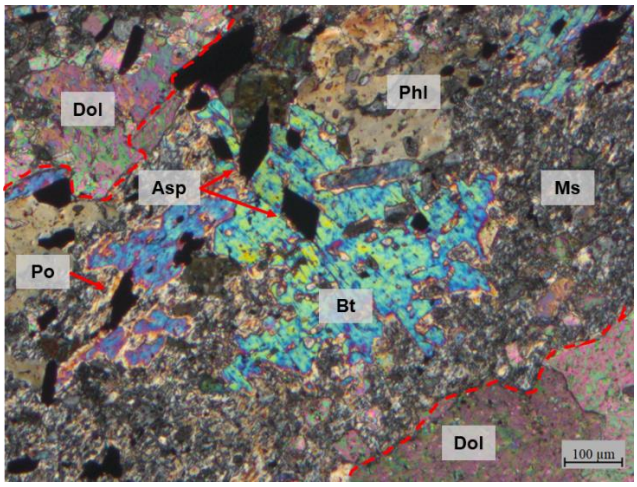


**Figure 6.** Sample SD69 under crossed nicols showing argillaceous layer (outlined by dashed red line) within dolomitic impure carbonate unit. Note biotite-phlogopite-sulphide associations and fine-grained muscovite-dolomite aggregates. Abbreviations: Asp = arsenopyrite; Bt = biotite; Dol = dolomite; Ms = muscovite; Phl = phlogopite; Po = pyrrhotite.

## 5 Future work

Zonation of ore-stage carbonate group minerals and chemical variations of white mica proximal and distal to ore will be investigated further. Cross-cutting relationships and chemical composition of carbonates will be assessed with cathodoluminescence (CL). Furthermore, drill core samples scanned at 26µm resolution have been submitted for complete geochemical characterization to ALS Global (results pending). Trace element associations will compliment hyperspectral interpretation of the alteration footprint and cooling trends within the system. In addition, protolith control on mineralization and alteration expression will be further constrained.

## Acknowledgements

Dr. Asinne Tshibubudze, School of Geosciences, University of Witwatersrand, is thanked for arranging funds for geochemical analyses for this project.

## References

Agus JL (2011) Mapping White Mica in Milled Prophyry Copper Pebbles Using Hyperspectral Imagery: An Exploration Study. MSc. Thesis Report. Faculty of Geo-Information Science and Earth Observation. University of Twente.

Clark RN (1999) Chapter 1: Spectroscopy of Rocks and Minerals, and Principles of Spectroscopy. Manual of Remote Sensing. Remote Sensing for the Earth Sciences 3:3-58.

Dalm M, Buxton MWN, van Ruitenbeek FJA (2017) Discriminating ore and waste in a porphyry copper deposit using short-wave infrared (SWIR) hyperspectral imagery. Mineral Engineering 105:10-18.

Laukamp C, Termin KA, Pejcic B, Haest M, Cudahy T (2012) Vibrational spectroscopy of calcic amphiboles - applications for exploration and mining. European Journal of Mineralogy 24: 863-878.

Masurel Q, Miller J, Hein KAA, Hanssen E, Thebaud N, Ulrich S, Kaisin J, Tessougue S (2016) The Yatela gold deposit in Mali, West Africa: The final product of a long-lived history of hydrothermal alteration and weathering. Journal of African Earth Sciences 113:73-87.

Masurel Q, Thebaud N, Miller J, Ulrich S, Hein K A.A, Cameron G, Beziat D, Bruguier O, Davis J (2017) Sadiola Hill: A World-Class Carbonate-Hosted Gold Deposit in Mali, West Africa. Economic Geology 112:23-47.

Kokaly RF, Clark RN, Swayze GA, Livo KE, Hoefen TM, Pearson NC, Wise RA, Benzel WM, Lowers HA, Driscoll RL, Klein AJ (2017) USGS Spectral Library Version 7 Data: U.S. Geological Survey data release, https://dx.doi.org/10.5066/F7RR1WDJ

Roache TJ, Walshe JL, Huntington JF, Quigley MA, Yang K, Bil BW, Blake KL, Hyvarinen T (2011) Epidote-clinozoisite as a hyperspectral tool in exploration for Archean gold. Australian Journal of Earth Sciences 58:813-822.

Van Ruitenbeek, FJA, Cudahy, T, Hale, M, van der Meer, FD (2005) Tracing fluid pathways in fossil hydrothermal systems with near-infrared spectroscopy. Geology 33(7):597–600.

van Ruitenbeek, FJA, Cudahy TJ, van der Meer FD, Hale M (2012) Characterization of the hydrothermal systems associated with Archean VMS-mineralization at Panorama, Western Australia, using hyperspectral, geochemical and geothermometric data. Ore Geology Reviews 45:33-46.

van Ruitenbeek, FJA, van der Werff HMA, Bakker WH, an der Meer FD, Hecker CH, Hein KAA (2017) Rapid classification of infra-red hyperspectral imagery of rocks with decision trees and wavelength images. http://www.itc.nl/library/papers_2017/pres/vanruitenbeek_rap_ppt.pdf

Wang R, Cudahy T, Laukamp C, Walshe JL, Bath A, Mei Y, Young C, Roache TJ, Jenkins A, Roberts M, Barker A, Laird J (2017) White Mica as a Hyperspectral Tool in Exploration for the Sunrise Dam and Kanowna Belle Gold Deposits, Western Australia. Economic Geology 112:1153-1176